INTERNATIONAL JOURNAL FOR NUMERICAL METHODS IN FLUIDS
Int. J. Numer. Meth. Fluids 2001; **36**: 165–184

Numerical study of flows with multiple free surfaces

P. K. Mohapatra[a], S. Murty Bhallamudi[b,*] and V. Eswaran[c]

[a] *National Institute of Hydrology, Roorkee, India*
[b] *Department of Civil Engineering, Indian Institute of Technology Madras, India*
[c] *Department of Mechanical Engineering, Indian Institute of Technology Kanpur, India*

SUMMARY

This paper demonstrates that a numerical method based on the generalized simplified marker and cell (GENSMAC) flow solver and Youngs' volume of fluid (Y-VOF) surface-tracking technique is an effective tool for studying the basic mechanics of hydraulic engineering problems with multiple free surfaces and non-hydrostatic pressure distributions. Two-dimensional flow equations in a vertical plane are solved numerically for this purpose. The numerical results are compared with experimental data and earlier numerical results based on a higher-order depth-averaged flow model available in the literature. Two classical problems, (i) flow in a free overfall and (ii) flow past a floor slot, are considered. The numerical results correspond very well with the experimental data for both sub-critical and supercritical flows. Copyright © 2001 John Wiley & Sons, Ltd.

KEY WORDS: GENSMAC; multiple free surface flow; surface tracking; Y-VOF

1. INTRODUCTION

Free surface flows are defined as the flows where one or more of the boundaries is not physically constrained but can adjust to conform to the flow condition [1]. In unsteady free surface flows, the location of the free surface changes continuously as the solution progresses and its evolution has to be determined. In the case of steady free surface flows, the free surface is not known *a priori* and the objective is to locate it correctly. The quantitative description of such problems depends on successfully locating the free surface.

Principles of shallow water theory [2,3] cannot be used to simplify the analysis of many free surface flow problems when the streamline curvature is not small and a non-hydrostatic pressure distribution exists. Examples of such flows in hydraulic engineering are (1) the flow over a spillway, (2) dam-break flow, (3) a hydraulic jump, (4) the flow past a floor slot, etc.

* Correspondence to: Department of Civil Engineering, Indian Institute of Technology Madras, Chennai 600 036, India.

Received July 1999
Revised November 1999

In the past, several higher-order depth-averaged models have been developed for the analysis of free surface flows by considering the effect of non-hydrostatic pressure distribution [4–7]. However, these methods are based on certain assumptions for the flow structure, i.e., the velocity and the pressure distribution in the vertical direction. Therefore, these methods may not be applicable to general free surface flow problems (e.g., flows with multiple free surfaces).

Two-dimensional flow equations in a vertical plane can be numerically solved for a detailed study of the mechanics of the free surface flows without having to make any simplifying assumptions regarding the flow structure. The marker-and-cell (MAC) method by Harlow and Welch [8] was the first method in this regard. In this method, massless marker particles are introduced in all the cells initially containing the fluid. A Lagrangian approach is used to determine the later positions of these particles and hence the location of the free surface. The simplified marker-and-cell (SMAC) method of Amsden and Harlow [9] significantly improved the computational efficiency of the MAC method. In this method, the cycle for the flow field computation is divided into two parts, one to predict the velocity field and the other to correct the velocity and pressure fields to satisfy continuity. Many modifications to the original SMAC method have appeared in literature in recent years [10–14]. All these methods attempt to improve the computational efficiency of the SMAC method by adapting better numerical techniques for solving the pressure field and more efficient algorithms for surface tracking.

Different techniques have also been developed for free surface tracking. Notable among them is the SOLA-VOF method by Hirt and Nichols [15] in which the 'volume of fluid' (VOF) technique is used for surface tracking with solution algorithm (SOLA) from MAC method. This method uses a simple mass balance equation for time stepping a variable F, defined as the fractional volume of the cell occupied by the fluid. Youngs (Y) [16] presented a refined VOF technique based on the geometry of the orientation of the neighboring surface cells. Rudman [17] has recently shown that the Y-VOF technique of Youngs is generally superior to the other techniques for surface tracking.

Although MAC and VOF techniques are specially designed for solving free surface flows, their application to problems of interest in hydraulic engineering is only recent. Strelkoff [18] reported an exploratory numerical study on dam-break flow for dry bed conditions using the VOF technique. Qingchao and Drewes [19] used the same technique in their turbulence flow model for free and forced hydraulic jumps. Lemos and Martins [20] have also used the VOF technique in their numerical study of the impact of solitary waves on obstacles. Bradford and Katopodes [21] developed a non-hydrostatic turbulence model for overland flow using the modified MAC method of Tang [22]. Stansby and Zhou [23] developed a two-dimensional turbulence solver for flows with non-hydrostatic pressure distribution. They used a numerical technique similar in spirit to the SMAC method for solving the governing equations and a height function method for free surface tracking. Recently, the present authors [24] have adapted a hybrid technique which combined the GENSMAC Navier–Stokes solver [11] with the Y-VOF technique [18] to study the effect of non-hydrostatic pressure distribution on the dam-break flow.

One of the unique advantages of these VOF techniques over other methods, such as the height function method, is their ability to track multiple free surfaces in a convenient way. The robustness of the VOF techniques allows them to solve a spectrum of problems not accessible to most other surface-tracking methods. Although these methods have become very popular

and are adopted in many commercial software packages, the above feature of the VOF techniques has not been exploited to study the basic mechanics of hydraulic engineering problems with multiple free surfaces. All the works cited above involve steady and unsteady flow problems with only one free surface. Our aim in this paper is to assess the applicability of the Y-VOF technique [17] to more complicated problems involving multiple free surfaces. We have chosen two classical open channel flow problems, (1) a free overfall (two free surfaces) and (2) the flow past a floor slot (three free surfaces), for this purpose. The applicability of the method is tested by comparing the present numerical solutions with the experimental data and with previous numerical results available in literature.

2. FORMULATION

2.1. Governing equations

As our focus is on basic mechanics and surface tracking, we have chosen for study two problems where the inertial and gravity effects are dominant and the turbulence effects are minor. The governing equations for these two-dimensional incompressible inviscid flows in a vertical plane are

$$\frac{\partial u}{\partial x}+\frac{\partial v}{\partial y}=0 \tag{1}$$

$$\frac{\partial u}{\partial t}+\frac{\partial u^2}{\partial x}+\frac{\partial uv}{\partial y}=-\frac{1}{\rho}\frac{\partial p}{\partial x}+g_x \tag{2}$$

$$\frac{\partial v}{\partial t}+\frac{\partial uv}{\partial x}+\frac{\partial v^2}{\partial y}=-\frac{1}{\rho}\frac{\partial p}{\partial y}+g_y \tag{3}$$

In the above equations, u and v are the velocities in the x- and y-directions respectively, p is the pressure, g_x and g_y are gravity components in the x- and y-directions respectively and ρ is the density. The co-ordinate axes x and y are in the horizontal and the vertical directions respectively.

2.2. Numerical method

Various numerical methods are available in the literature for solving Equations (1)–(3) for free surface conditions. In an earlier study [24] we adapted a numerical method that is a hybrid of the GENSMAC Navier–Stokes solution method [11] and the Y-VOF surface-tracking technique [17] for studying the dam-break flow problem. The same numerical method is used herein to solve the governing equations (1)–(3). Therefore, only a brief outline is given below.

A typical finite difference cell arrangement is shown in Figure 1. In this figure, 'F' indicates a full cell, 'S' indicates a surface cell, 'E' indicates an empty cell and 'B' indicates a boundary cell. The velocities are specified at the cell faces while the pressure is specified at the cell center. The velocity field $\tilde{u}_{i,j}$ and $\tilde{v}_{i,j}$, the pressure field $\tilde{\phi}_{i,j}$, and the position of the free surface h_i, are

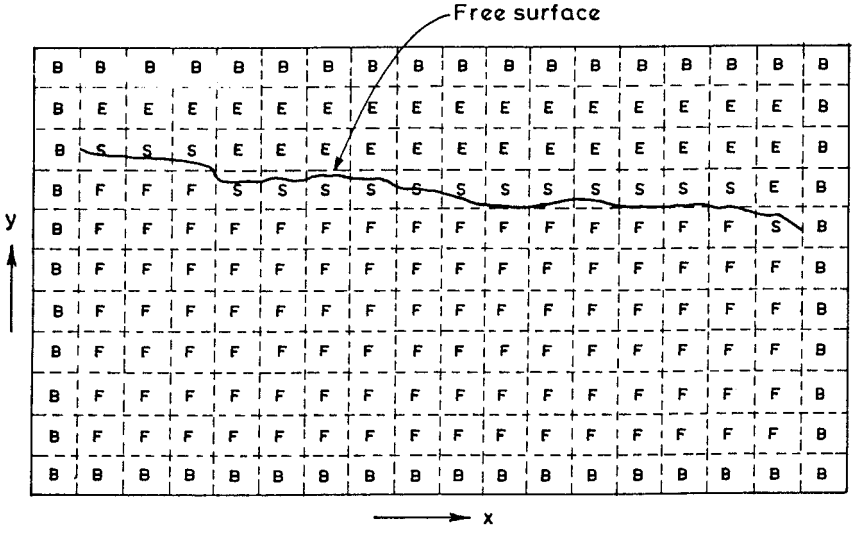

Figure 1. Computational mesh.

known at any time-level t (either from a previous time level computation or as initial conditions at t_{ini}). The velocity and pressure fields are determined for the new time level $t + \Delta t$, using the finite difference form of the governing equations and the following procedure.

STEP 1. An arbitrary pressure field $\phi_{i,j}$ is assumed as the new time level values at the interior points while ensuring the correct specification of the pressure, i.e., atmospheric pressure for the surface cells.

STEP 2. A velocity field $\hat{u}_{i,j}$ and $\hat{v}_{i,j}$ is predicted for time $t + \Delta t$ by explicitly solving the finite difference form of the momentum equations (2) and (3) using the known velocities $\tilde{u}_{i,j}$ and $\tilde{v}_{i,j}$ at time t and the assumed pressure field $\phi_{i,j}$. For this purpose, unlike in the SMAC or GENSMAC method, upwinding is introduced in the present numerical model while finite differencing the convective terms. The pressure and the transient terms are forward differenced.

Finite difference equations can be applied to determine the velocities only for the internal cells. Velocities for the boundary and surface cells are calculated by applying the boundary conditions. On the inflow boundary, both $\hat{u}_{i,j}$ and $\hat{v}_{i,j}$ are prescribed. At the outflow section, 'convective outflow' boundary conditions are applied. On the solid boundary, the appropriate boundary condition for the Euler equations, the free slip condition is applied. This condition is implemented by using a reflection technique. As in the SMAC method the tangential stress condition and the continuity equation are applied to obtain the surface cell velocities.

STEP 3. The predicted velocity field from Step 2 is then corrected to obtain a final velocity field, which satisfies the continuity equation. For this purpose, a Poisson equation for the pressure correction, ψ as given below, is solved

$$\frac{\partial^2\psi}{\partial x^2}+\frac{\partial^2\psi}{\partial y^2}=\frac{\partial\hat{u}}{\partial x}+\frac{\partial\hat{v}}{\partial y} \tag{4}$$

As in the GENSMAC algorithm [11], the conjugate gradient (CG) method is used in this study for solving Equation (4), discretized using center differences. The boundary condition for solving Equation (4) is a homogeneous *Neumann condition* at the solid boundary, the inlet and the outlet, as correct normal velocities are known at these boundaries. It is a homogeneous *Dirichlet condition* at the free surface because correct pressure is specified on this boundary. Corrected velocities at $t+\Delta t$ are obtained using the following equations:

$$u_{i,j}=\hat{u}_{i,j}-\frac{\partial\psi}{\partial x}, \qquad v_{i,j}=\hat{v}_{i,j}-\frac{\partial\psi}{\partial y} \tag{5}$$

STEP 4. Surface tracking is then done with the new velocity field to obtain the new free surface location. It is computed using the mass balance equation for the fraction of the cell filled with fluid, F

$$\frac{\partial F}{\partial t}+\frac{\partial Fu}{\partial x}+\frac{\partial Fv}{\partial y}=0 \tag{6}$$

Equation (6) is not solved by the usual finite difference approach in order to limit the numerical diffusion. Fluxes are first computed for all the cells using first-order upwinding. The outward fluxes for all the surface cells are then refined using the orientation of the free surface within the cell, which depends upon the F values in all the neighboring cells. We followed the Y-VOF technique [17] for this purpose.

3. RESULTS AND DISCUSSION

The numerical model presented in the previous section is used, in a false transient approach, to study (1) the steady flow in a free overfall and (2) the flow past a floor slot. Both sub-critical and supercritical flows are considered in this study.

3.1. Free overfall

The main objective of the present study is to demonstrate the applicability of the Y-VOF technique for a detailed analysis of hydraulic engineering problems involving multiple free surfaces. We have chosen the free overfall as a case study because (i) it has two free surfaces and (ii) extensive experimental data [25–27] is available in the literature with which the applicability of the numerical model can be assessed. Analytical solutions based on the potential flow assumption [28–31] are also available for this problem. Recently, Khan and Steffler [7] used a finite element method to solve the vertically averaged moment equations for this problem. The strengths and limitations of the above higher-order depth-averaged model can be also assessed.

The definition sketch of a free overfall is presented in Figure 2. A free overfall with a horizontal frictionless bed and a vertical drop is considered. The pressure distribution in the

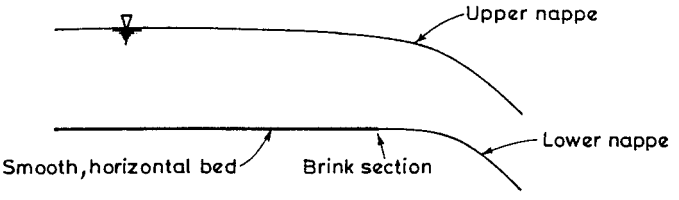

Figure 2. Definition sketch for a free overfall.

vertical direction for this case is non-hydrostatic. We solve the two-dimensional flow equations in a vertical plane to obtain (i) the end-depth ratio (ratio of brink depth to critical depth), (ii) the water surface profile, the pressure distribution and the velocity distribution on the upstream side of the overfall, and (iii) the lower and upper nappe profiles of the free jet.

The computational domain for the numerical solution of the free overfall problem is shown in Figure 3. In this figure, ABC is the inflow section (AB = 0.2 m, BC = 0.15 m), ED is the outflow section (= 0.35 m) and BF is the channel bed (= 0.8 m). The total length of the domain in the x-direction, i.e., CD = AE = 0.95 m. For given flow depth, BG, and the discharge at the inflow section, it is required to determine the water surface profile, GJ, on the upstream side of the free overfall, the upper nappe profile, JH, and the lower nappe profile, FI, as part of the solution. It is also required to compute the complete velocity and pressure distributions. For this purpose, the computational domain ACDE is discretized into rectangular cells, with $\Delta x = 5$ mm and $\Delta y = 5$ mm. The initial upper water surface profile is taken as horizontal passing through the point G, BG being the specified inflow depth. The initial lower nappe profile is taken as a horizontal continuation of the channel bed, BF. The initial horizontal velocity u for all the full cells is taken equal to the given horizontal velocity at the inflow section. The initial vertical velocity v for all the full cells is taken equal to zero. With

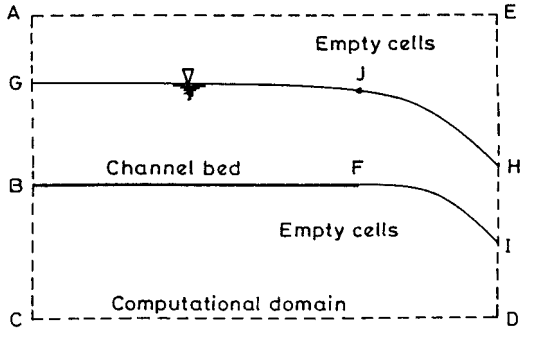

Figure 3. Computational domain for the free overfall.

the above arbitrary initial conditions, the numerical model is run in a false transient setting to determine the correct steady state solution corresponding to the given inflow depth and discharge. While doing so, the depth and the velocity at the inflow boundary are kept constant at all times. Convective outflow boundary conditions are applied at the outflow boundary. The numerical solution is assumed to have attained the steady state when

$$\left|\Gamma(t+\Delta t)-\Gamma(t)\right| \leq \varepsilon \tag{7}$$

where Γ represents all dependent variables (u, v and F) and $\varepsilon = 0.00001$.

3.1.1. Sub-critical flow. For the case of sub-critical flow, the inflow depth and discharge are equal to 0.132 m and 0.14307 $m^3 s^{-1} m^{-1}$ respectively. The computed water surface profile obtained for this case is compared with the experimental results [26] in Figure 4. Both lower and upper nappes of the outcoming free jet are shown in this figure. The computed results match well with the experimental data. The end depth (which is an important parameter in the discharge estimation) is predicted very well by the present numerical method, with an error of only 4 per cent.

Figure 5 shows the profile of the bed pressure upstream of the brink. In this figure the non-dimensional bed pressure at any section, $p_b/\rho gh$ (p_b = bed pressure, h = flow depth at the section) is shown versus the non-dimensional distance from the brink, x/h. As can be seen from this figure, the present numerical results compare well with (i) the experimental results [26] and (ii) with previous numerical results obtained by Khan and Steffler [7] using the vertically averaged moment (VAM) equations. Although the results obtained by Khan and Steffler are marginally better, the maximum error in the present simulations is only 5.4 per cent. The present numerical model slightly overestimates the flow depth and therefore the non-dimensional bed pressure is underestimated. Figure 6 plots the non-dimensional pressure distribution at the brink section, $p/\rho gh_b$ (h_b = flow depth at the brink) versus the non-dimensional height above the bed, y/h_b. In this figure, the pressure distribution obtained using

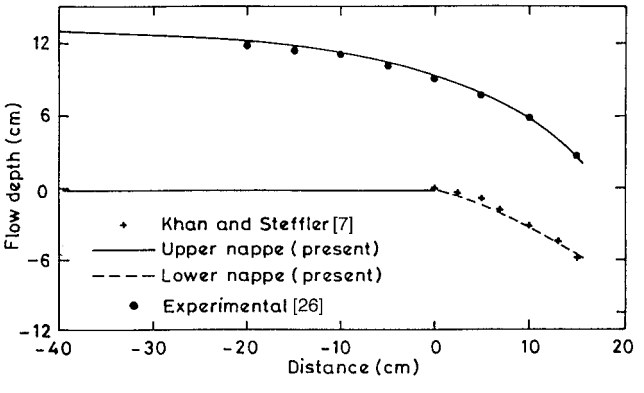

Figure 4. Free surface profile in a free overfall: sub-critical flow.

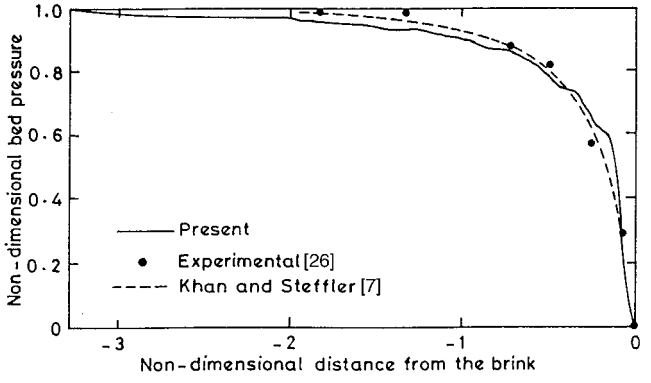

Figure 5. Bed pressure profile in a free overfall: sub-critical flow.

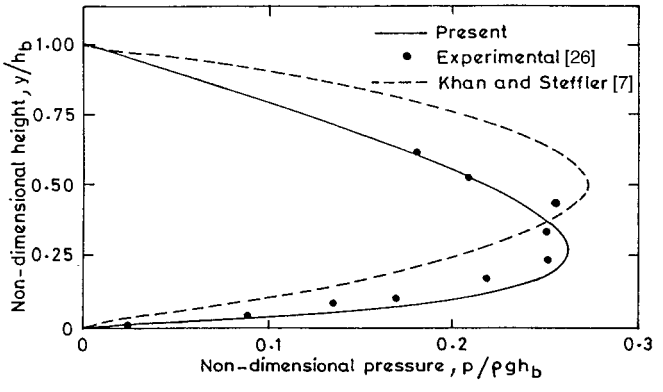

Figure 6. Pressure distribution at the brink section: sub-critical flow.

the present numerical method, by Khan and Steffler [7] and experimentally by Rajaratnam and Muralidhar [26] are compared. It can be seen from this figure that although the VAM model used by Khan and Steffler [7] simulates the maximum pressure accurately (error = 3.1 per cent) its prediction of the profile is not satisfactory. This is due to the limitations of the *a priori* assumptions made while deriving the VAM equations. On the other hand, the present numerical model does not assume any pressure or velocity distribution and so simulates the vertical distribution of the pressure satisfactorily (Figure 6). The error in our simulated maximum pressure is only 1.73 per cent. The difference in locating the maximum pressure is $0.037h_b$, which is much less than $0.213h_b$ obtained in the VAM model application.

Figure 7 shows a comparison of the computed horizontal velocity profile at the brink with those obtained from the two-dimensional potential flow model developed by Montes [32] and by Khan and Steffler [7]. In this figure, the non-dimensional horizontal velocity, u/u_c

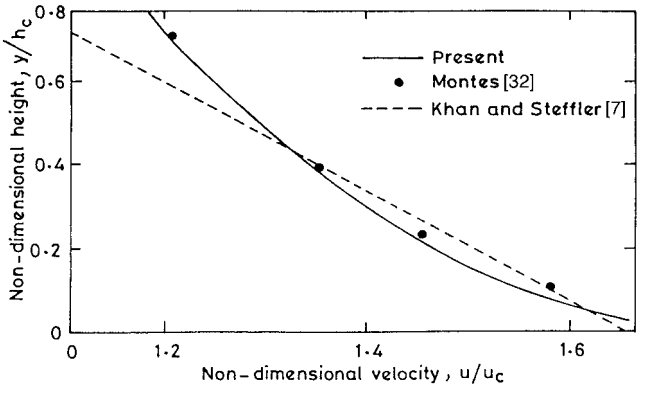

Figure 7. Horizontal velocity profile at the brink section: sub-critical flow.

(u_c = critical velocity for the given flow rate) is plotted versus the non-dimensional distance above the bed, y/h_c (h_c = critical depth for the given flow rate). As the governing equations (1)–(3) do not include the viscous terms and the specified flow at the inflow boundary is irrotational, the computed results using the present model should match with the potential flow solution of Montes [32], which is the case (as indicated by Figure 7). The maximum difference between the solution of Montes [32] and the present solution is only 2.3 per cent. On the other hand, the agreement between the result obtained using the VAM model and the potential flow solution is not as good. The VAM model makes an *a priori* assumption that the horizontal velocity distribution is linear, which is appropriate for the flow sections upstream of the brink but breaks down at the brink section. Figure 8 shows the computed and measured non-dimensional vertical velocity, v/u_c at the brink section versus the non-dimensional height

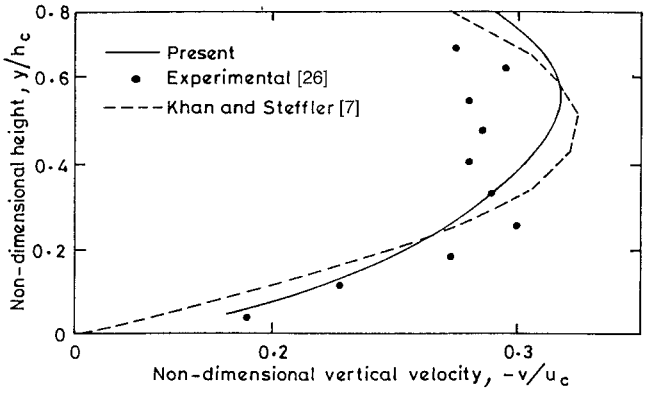

Figure 8. Vertical velocity profile at the brink section: sub-critical flow.

above the bed, y/h_c. While there is agreement between the present numerical results and those obtained by Khan and Steffler [7], both numerical results do not match that well with the experimental data (maximum error = 12.6 per cent), particularly at locations far above the bed i.e., for $y/h_c > 0.35$. However, the general trend of the vertical velocity variation is simulated satisfactorily by the present as well as the VAM model.

3.1.2. Supercritical flow. The experimental data for the free overfall with a supercritical upstream flow is taken from the plots presented by Marchi [30]. Figure 9 shows the computed and measured water surface elevation and the lower nappe profile of the free jet. The agreement between the numerical and experimental results is excellent (maximum error < 0.5 per cent), which indicates that the present numerical model is capable of simulating both sub- and supercritical flow conditions. It may be noted here that the end depth ratio for a supercritical flow is different from that for a sub-critical flow. Unlike in the sub-critical flow, where the control section is at the downstream end, the control section is at the upstream end for a supercritical flow. Results for the pressure and velocity distributions can be obtained by the present numerical method. However, these results are not shown here as no experimental results are available for comparison.

3.2. Flow past a floor slot

The definition sketch for the flow past a floor slot is shown in Figure 10. We have chosen this as a case for demonstrating the applicability of the present model because (i) it is more complicated than a free overfall, and has three free surfaces; (ii) the height function methods for surface tracking, and the higher-order depth-averaged flow models become very complicated in this case; and (iii) extensive experimental data is available in the literature, with which the model accuracy can be assessed.

Studies concerning the flow past a floor slot are few. In fact, we are not aware of any numerical solutions of this problem. Venkatraman [33] studied the slot flow problem analytically. He assumed a hydrostatic pressure distribution and a uniform velocity profile to find

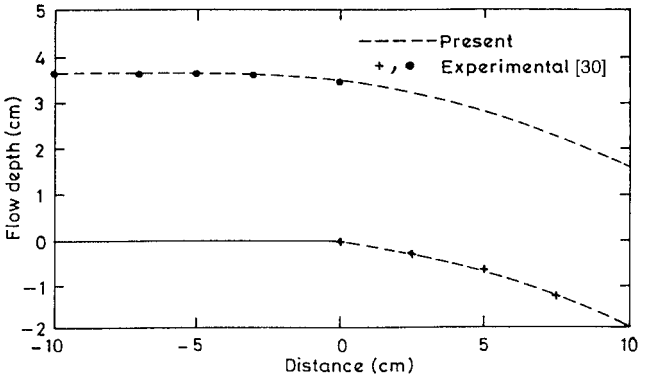

Figure 9. Free surface profile in a free overfall: supercritical flow.

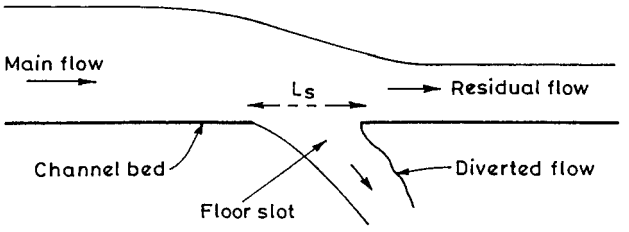

Figure 10. Definition sketch for flow past a floor slot.

expressions for the angle of diverted jet and the ratio of water depths. Nasser *et al.* [34] presented theoretical and experimental results for the values of the coefficient of discharge for the lateral outflow. The ratio of the diverted flow to the main flow as a function of the slot parameters was also presented. However, the equation for the coefficient of discharge is semi-empirical in nature and requires an empirical correction to the head driving the flow to account for streamline curvature. Ramamurthy and Satish [35] experimentally studied the effect of the ratio of slot width to flow depth on the slot discharge, and measured the pressure and velocity distributions at different locations.

In this section, the numerical model is used to simulate the flow field of the flow past a floor slot. The computed results are compared with the experimental data obtained by Ramamurthy and Satish [35]. The numerical simulations are then used to determine the discharge characteristics as a function of the slot width and the inflow velocity head. In all the simulations reported here, the bed is assumed to be frictionless and horizontal. The computational domain (Figure 11) is 6 m long in the x-direction (AB = CD = 6 m) and 1.7 m high in the y-direction (AD = BC = 1.7 m). The channel bed, EFGH is located at a height of 0.5 m above the bottom of the computational domain (AE = BH = 0.5 m). The slot, FG, is situated at a distance of 4.6

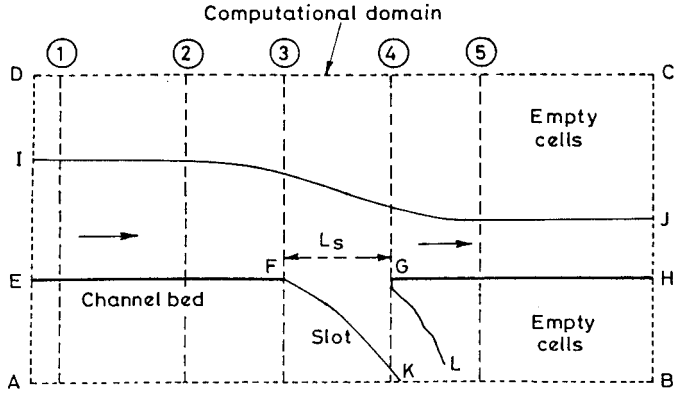

Figure 11. Computational domain for flow past a floor slot.

m from the inflow section (EF = 4.6 m). For given slot width, FG, inflow depth, EI, and the discharge at the inflow section, it is required to determine the water surface profile, IJ, above the channel bed, and the profile of the jet, FK–GL, issuing out of the slot, as part of the solution. It is also required to compute the complete velocity and pressure distributions. For this purpose, the computational domain ABCD is discretized into rectangular cells, with $\Delta x = 6.2$ mm and $\Delta y = 6.2$ mm. The initial and the boundary conditions applied are similar to those described for the overfall problem.

For the first set of results [35], the input data is the inflow discharge, $q_0 = 0.1378$ m^2 s^{-1}, the slot width, FG = $L_s = 19.1$ mm, and the inflow depth, EI = $h_0 = 80$ mm. Figures 12–16 present the vertical pressure distribution at cross-sections 1, 2, 3, 4 and 5 (see Figure 11) respectively. The pressure distributions obtained numerically using the present model, experimentally by

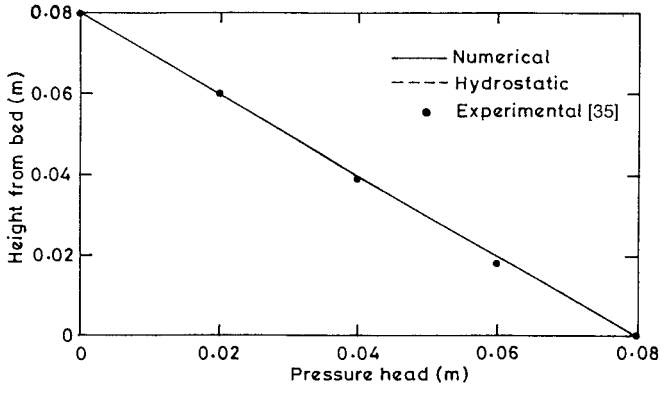

Figure 12. Pressure distribution at section 1: flow past a floor slot.

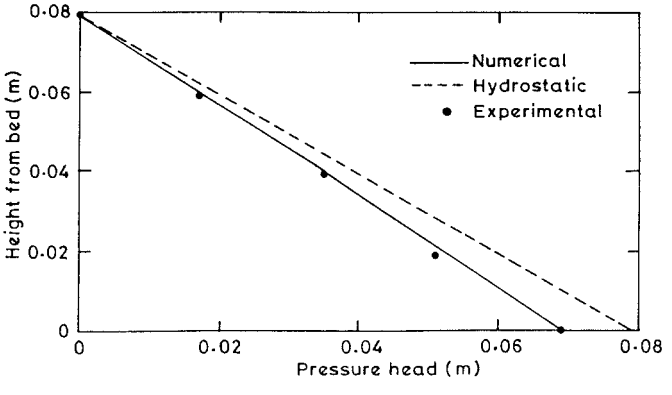

Figure 13. Pressure distribution at section 2: flow past a floor slot.

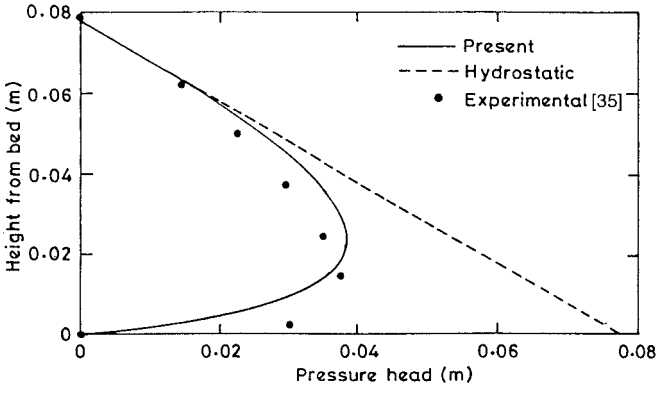

Figure 14. Pressure distribution at section 3: flow past a floor slot.

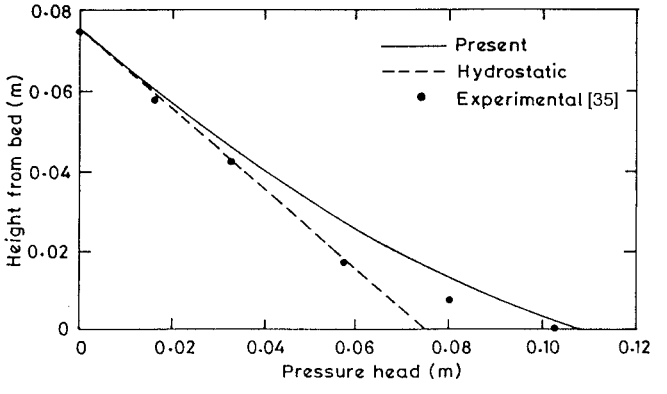

Figure 15. Pressure distribution at section 4: flow past a floor slot.

Ramamurthy and Satish [35] and using the hydrostatic assumption based on the computed water surface profile are presented in these figures. The numerically simulated pressure distribution agrees very well with the experimental data. It can be clearly seen that the pressure distribution is hydrostatic at sections 1 and 5 (Figures 12 and 16), which are far from the slot and where the vertical velocity component is close to zero. The present numerical model simulates this almost exactly. The pressure is far from the hydrostatic value at sections 2, 3 and 4 (Figures 13–15), which are in the vicinity of the slot. As indicated by the experiments (Figure 13), the actual pressure at section 2 is less than the corresponding hydrostatic value due to convex streamline curvature. This non-hydrostatic pressure distribution is simulated excellently by the present numerical model, the maximum error being only 1 per cent. The surface and the floor pressures at section 3 (Figure 11) just at the beginning of the slot should be atmospheric,

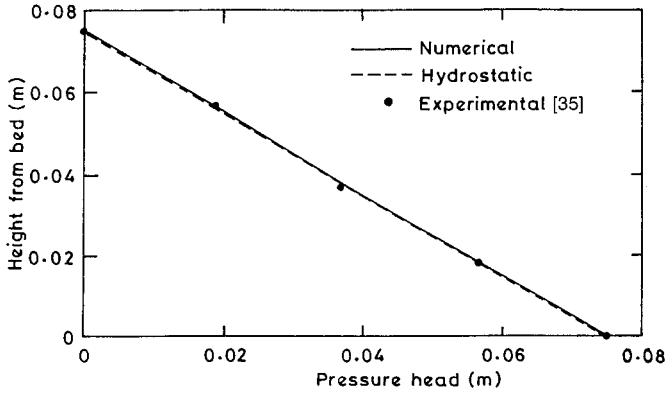

Figure 16. Pressure distribution at section 5: flow past a floor slot.

and a maximum pressure value should occur slightly above the bed. Experimental data (Figure 14) do indicate this. The present numerical model simulates this slot effect satisfactorily. Error in the simulated value for maximum pressure is only 2.6 per cent and the difference in the simulated and observed locations for the maximum pressures is $0.105h_3$ ($h_3 =$ flow depth at section 3). Section 4 is located slightly downstream of the slot end (Figure 11) and there is an occurrence of a stagnation point in the vicinity of the floor point of this section. Therefore, the floor pressure at this section is more than the corresponding hydrostatic value, as indicated in Figure 15. This stagnation effect is simulated satisfactorily by the present numerical model, the error in the floor pressure simulation being only 5.8 per cent.

Figures 17–21 present the horizontal velocity distributions at sections 1, 2, 3, 4 and 5 respectively. In the numerical model, the bed is assumed to be frictionless and therefore a

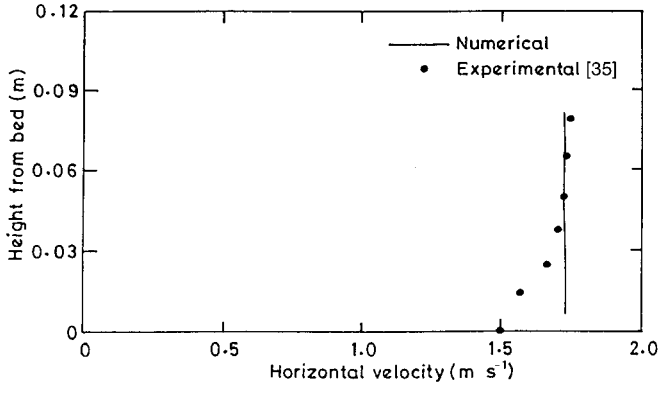

Figure 17. Horizontal velocity at section 1: flow past a floor slot.

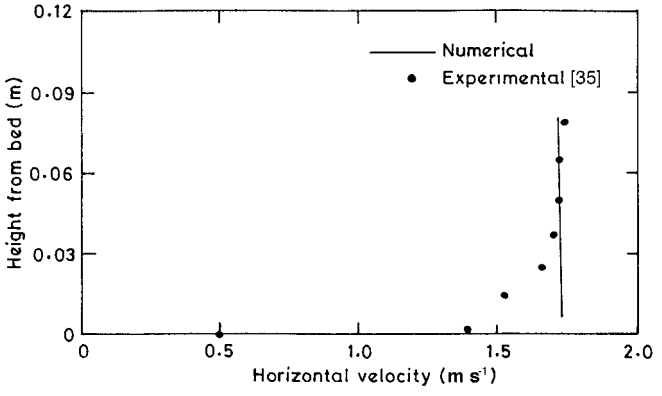

Figure 18. Horizontal velocity at section 2: flow past a floor slot.

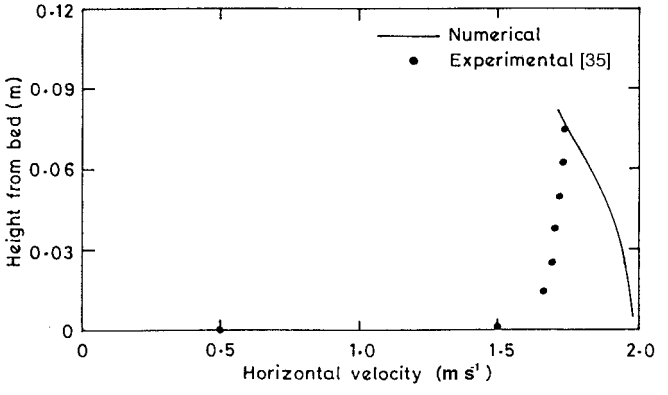

Figure 19. Horizontal velocity at section 3: flow past a floor slot.

free-slip boundary condition is applied at the bed. This introduces error and hence the agreement between the observed and simulated velocity profiles is not good. Although upstream of the slot the error due to friction effects is confined to a region close to the bed (Figures 17 and 18), this has a significant effect on the velocity profiles near the slot (Figures 19 and 20). Better performance by the model would require inclusion of a turbulence model.

In hydraulic engineering practice, floor slots are typically used (i) to divert water from one channel to another, (ii) as horizontal trash racks in hydro power plants, and (iii) as outlets in streets. In all these applications, it is very important to estimate the discharge through the slot, which depends on the inflow characteristics and the slot width. In the second set of results for the flow past a floor slot, these effects are quantified using non-dimensional parameters. Figure 22 presents the effect of inflow characteristics on the coefficient of discharge, C_d, defined by the following equation:

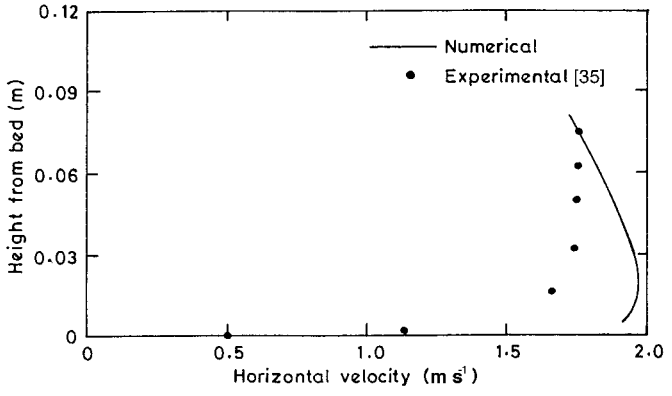

Figure 20. Horizontal velocity at section 4: flow past a floor slot.

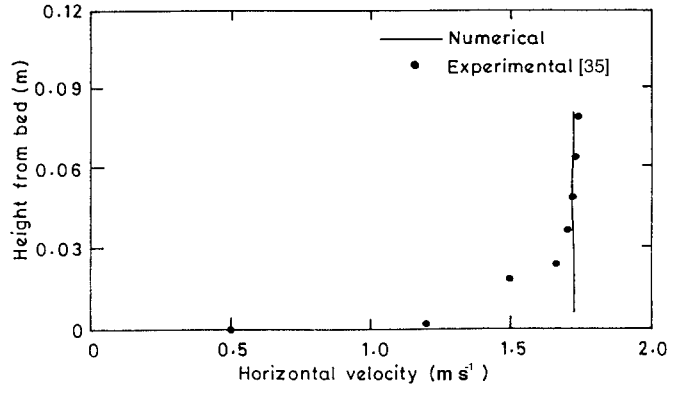

Figure 21. Horizontal velocity at section 5: flow past a floor slot.

$$q_s = C_d L_s \sqrt{2gE_3} \tag{8}$$

where q_s = discharge through the slot and E_3 = specific energy at the entrance section to the slot. Figure 22 shows the variation of C_d as a function of the non-dimensional velocity head at the entrance to the slot, i.e., $V_3^2/(2gE_3)$, where V_3 = average velocity at the entrance to the slot. Non-linear regression equation based on results from more than 20 numerical runs is used to plot the curve in this figure. The input data for these runs are taken from Nasser *et al.* [34], and the range of variables tested is shown in Table I.

The ratio L_s/h_3 of the slot width, L_s, to the flow depth at the entrance section, h_3, also affects the C_d but is not considered here and only a single regression curve is presented for the sake of simplicity. Figure 22 also shows the experimental data obtained by Nasser *et al.* [34]. It can

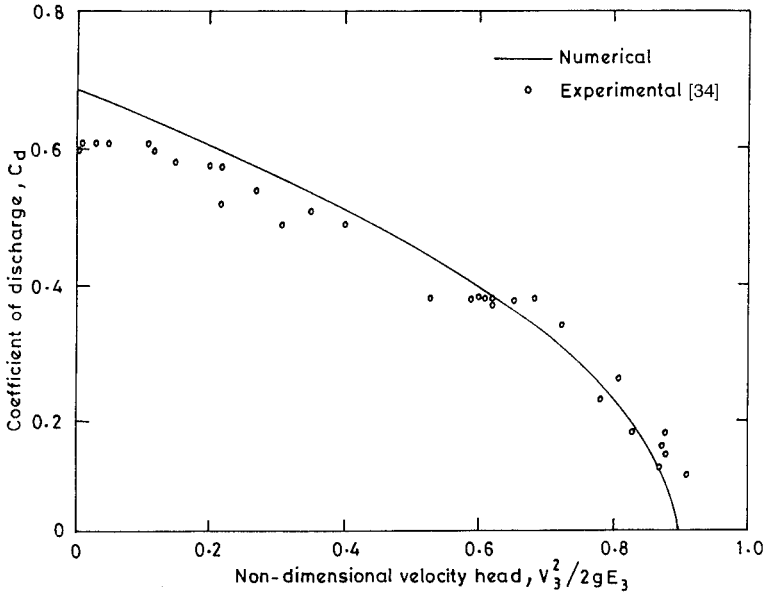

Figure 22. Variation of C_d with dimensionless velocity head: flow past a floor slot.

Table I. Variable values used in the floor slot problem.

L_s (cm)	q_0 (l s^{-1})	Fr
2, 3, 4, 5	10–25	1–3
5.1, 7.6, 12.7, 19.1	15–75	0.4–0.8

be clearly seen from this figure that, on the whole, the numerical model is able to compute the discharge characteristics of the slot quite well. The error in the maximum C_d value (corresponding to the hypothetical case of zero horizontal velocity condition) is 10.6 per cent. This is reasonable considering the fact that we have not included turbulence effects in our model. Also, this is mostly the extrapolation error in our regression analysis of 20 numerical results.

The discharge through the slot can also be parametrized using the ratio of slot width to the inflow critical depth. The computed results obtained in the numerical runs are analyzed in an alternative way to derive the curve presented in Figure 23. In this figure, performance factor $\eta_s = q_s/q_0$ is plotted as function of L_s/h_c, where h_c = inflow critical depth $\equiv (q_0^2/g)^{1/3}$. Figure 23 shows the numerically derived curve and the experimental data of Nasser *et al.* [34]. It can be seen from this figure that the numerical results agree well with the experimental data. The maximum difference between the experimental data and the corresponding numerically simulated value is only 8.5 per cent.

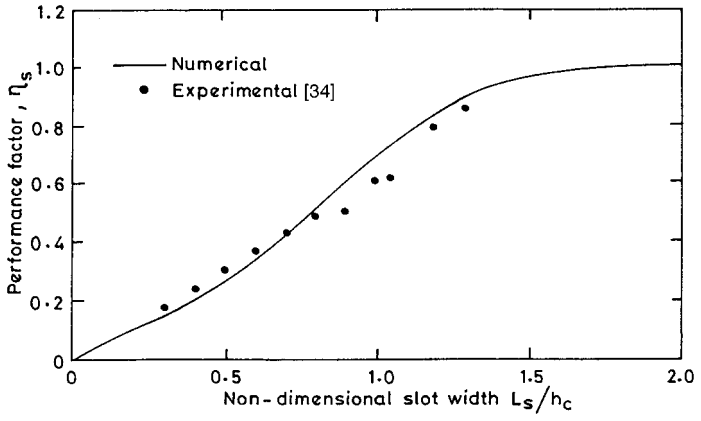

Figure 23. Variation of η_s with non-dimensional slot width.

For the sake of completeness, we show the numerically simulated water surface and jet profiles for a typical run in Figure 24. The velocity vectors in the vicinity of the slot are also shown in this figure. A typical run for the slot problem involves 1700 iterations, i.e., 1700 time steps in the false transient method, to obtain the steady flow field starting from the arbitrary initial conditions. The CPU time for one complete run was equal to 31 min 50 s on a HP Infinity 2000 machine with Pentium processor.

4. CONCLUSIONS

In this study, a numerical method based on the GENSMAC flow solver [11] and the Y-VOF surface-tracking technique [17] is used to simulate the two-dimensional flow in a free overfall and the flow past a floor slot. The numerical results for the steady flow in a free overfall are compared with experimental data and earlier numerical results based on VAM equations. The numerical results for the water surface profile match very well with the experimental data for both sub- and supercritical flows. The error in the estimation of the end depth ratio is only 4 per cent. The pressure and the velocity distributions at the brink section are also simulated satisfactorily by the present two-dimensional numerical model. The agreement between the present numerical results and experimental data for pressure distribution is better than that of the results obtained using the VAM model.

The present two-dimensional numerical results for the non-hydrostatic pressure distribution in the slot flow match well with the experimental data. The agreement between the numerical results and the experimental data, however, is not very good in the case of velocity distribution due to the inviscid flow assumption. However, the numerically derived values for the coefficient of discharge through the slot match well with the experimental data. The discharge characteristic of the slot as a function of non-dimensional slot width is also captured well.

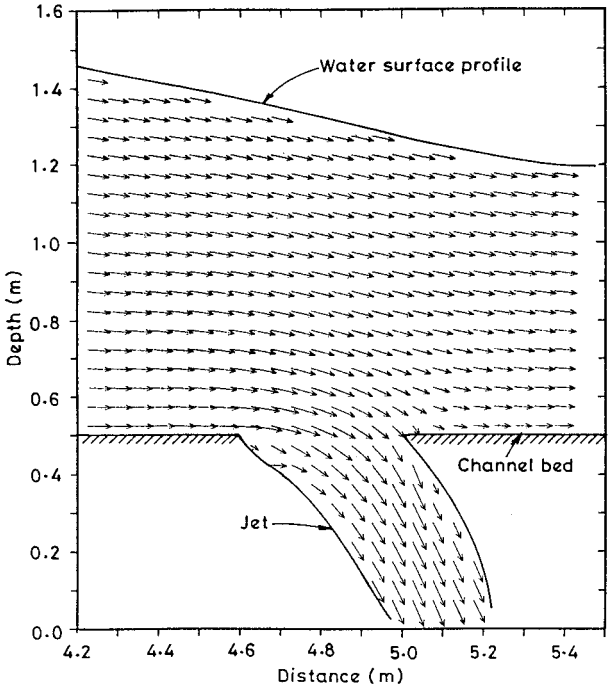

Figure 24. Free surface and jet profiles: flow past a floor slot.

The study demonstrates that the Y-VOF surface-tracking technique combined with the GENSMAC flow solver is an effective and robust tool for studying the basic mechanics of hydraulic engineering problems which involve multiple free surfaces and non-hydrostatic pressure. Such computations generate complete information about the flow field without making any a priori assumptions regarding the flow structure.

REFERENCES

1. Liggett JA. *Fluid Mechanics*. McGraw-Hill: New York, 1994; 393.
2. Cunge J, Holly FM, Verwey A. *Practical Aspects of Computational River Hydraulics*. Pitman: London, 1980.
3. Chaudhry MH. *Open Channel Flow*. Prentice-Hall: Englewood Cliffs, NJ, 1993.
4. Basco DR. Computation of rapidly varied, unsteady free-surface flow. US Geological Survey Report WRI 83-4284, 1983.
5. Gharangik A, Chaudhry MH. Numerical simulation of hydraulic jump. *Journal of Hydraulic Engineering, ASCE* 1991; **117**(9): 1195–1211.
6. Carmo JS, Santos FJ, Almeida AB. Numerical solution of the generalized Serre equations with the MacCormack finite-difference scheme. *International Journal for Numerical Methods in Fluids* 1993; **16**: 725–738.
7. Khan AA, Steffler PM. Modeling overfalls using vertically averaged and moment equations. *Journal of Hydraulic Engineering, ASCE* 1996; **122**(7): 397–402.
8. Harlow FH, Welch JE. Numerical calculation of time-dependent viscous incompressible flow. *The Physics of Fluids* 1965; **8**(12): 2182–2189.

9. Amsden AA, Harlow FH. *SMAC Method: A Numerical Technique for Calculating Incompressible Fluid Flows*. Los Alamos Scientific Laboratory, University of California: Los Alamos, NM, 1970.
10. Chen S, Johnson DB, Raad PE. The surface marker method. In *Computational Modeling of Free and Moving Boundary Problems*, *Vol. 1*. Proceedings of the 1st International Conference, 2–4 July, Southampton, UK, Wrobel LC, Brebbia CA (eds). CM Publications: Boston, 1993; 223–234.
11. Tome MF, McKee S. GENSMAC: a computational marker and cell method for free-surface flows in generalized domains. *Journal of Computational Physics* 1994; **110**(1): 171–186.
12. Nakayama T, Mori M. An Eulerian finite element method for time dependent free surface problems in hydrodynamics. *International Journal for Numerical Methods in Fluids* 1996; **22**: 175–194.
13. Armenio V. An improved MAC method (SIMAC) for unsteady high Reynolds free surface flows. *International Journal for Numerical Methods in Fluids* 1997; **24**: 185–214.
14. Chen S, Johnson DB, Raad PE, Fadda D. The surface marker and micro cell method. *International Journal for Numerical Methods in Fluids* 1997; **25**: 749–778.
15. Hirt CW, Nichols BD. Volume of fluid method for the dynamics of free boundaries. *Journal of Computational Physics* 1981; **39**: 201–225.
16. Youngs DL. Time-dependent multi-material flow with fluid distortion. *Numerical Methods for Fluid Dynamics* 1982; **4**(4): 337–360.
17. Rudman M. Volume-tracking methods for interfacial flow calculations. *International Journal for Numerical Methods in Fluids* 1998; **24**: 671–691.
18. Strelkoff T. Dam-break flood waves. In *Megatrends in Hydraulic Engineering*, Albertson ML, Papadakis CN (eds). Colorado State University: Fort Collins, 1986; 257–266.
19. Qingchao L, Drewes U. Turbulence characteristics in free and forced hydraulic jumps. *Journal of Hydraulic Research*, *IAHR* 1994; **32**(6): 877–898.
20. Lemos CM, Martins ML. A numerical study of the impact of solitary waves on obstacles of simple geometrical configuration. In *Advances in Fluid Mechanics*, *Vol. 9*. Proceedings of the 1st International Conference on Advances in Fluid Mechanics, Rahman M, Brebbia CA (eds). Computational Mechanics Publications: Southampton, UK, 1996; 113–123.
21. Bradford SF, Katopodes N. Nonhydrostatic model for surface irrigation. *Journal of Irrigation and Drainage Engineering*, *ASCE* 1998; **124**(4): 200–212.
22. Tang JH. Surge propagation on a porous bed. PhD thesis, University of Michigan, Ann Arbor, MI, 1991.
23. Stansby PK, Zhou JG. Shallow water flow solver with non-hydrostatic pressure 2D vertical plane problems. *International Journal for Numerical Methods in Fluids* 1998; **28**: 541–568.
24. Mohapatra PK, Eswaran V, Bhallamudi SM. Two-dimensional analysis of dam-break flow in vertical plane. *Journal of Hydraulic Engineering*, *ASCE* 1999; **125**(2): 183–192.
25. Rouse H. Discharge characteristics of the free overfall. *Civil Engineering* 1936; **6**(4): 257–260.
26. Rajaratnam N, Muralidhar D. Characteristics of the rectangular free overfall. *Journal of Hydraulic Research*, *IAHR* 1968; **6**(3): 233–258.
27. Rajaratnam N, Muralidhar D, Beltaos S. Roughness effects on rectangular free overfall. *Journal of Hydraulics Division*, *ASCE* 1976; **102**(5): 599.
28. Clarke NS. On 2-dimensional inviscid flow in a waterfall. *Journal of Fluid Mechanics* 1965; **22**(2): 359–369.
29. Strelkoff T, Moayeri MS. Pattern of potential flow in a free overfall. *Journal of Hydraulics Division*, *ASCE* 1970; **96**(4): 879–901.
30. Marchi E. On the free overfall. *Journal of Hydraulic Research*, *IAHR* 1993; **31**(6): 777–790.
31. Hager WH. Hydraulics of plane free overfall. *Journal of Hydraulic Engineering*, *ASCE* 1982; **109**(12): 1683–1697.
32. Montes JS. A potential flow solution for the free overfall. *Proceedings of the Institute of Civil Engineers*, *Water*, *Maritime and Energy* 1992; **96**: 259–266.
33. Venkataraman P. Divided flow in channels with bottom openings. *Journal of Hydraulics Division*, *ASCE* 1977; **103**(2): 190–194.
34. Nasser MS, Venkataraman P, Ramamurthy AS. Flow in a channel with a slot in the bed. *Journal of Hydraulic Research*, *IAHR* 1980; **18**(4): 359–367.
35. Ramamurthy AS, Satish MG. Discharge characteristics of flow past a floor slot. *Journal of Irrigation and Drainage Engineering*, *ASCE* 1986; **112**(1): 20–27.

